Available online at www.sciencedirect.com
ScienceDirect
Polymer 47 (2006) 7997–8012
polymer
www.elsevier.com/locate/polymer

A structure-based constitutive equation for filler-reinforced rubber-like networks and for the description of the Mullins effect

Bohumil Meissner*, Libor Matějka

Institute of Macromolecular Chemistry, Academy of Sciences of the Czech Republic, Heyrovský Square 2, 162 06 Prague 6, Břevnov, Czech Republic

Received 4 May 2006; received in revised form 9 September 2006; accepted 19 September 2006
Available online 10 October 2006

Abstract

A constitutive equation for elastomeric networks (ABGIL) was proposed by us previously and tested with a good success (Polymer 2003, 2004). It incorporates the Arruda and Boyce connectivity term based on Langevin statistics, the constraint term based on a generalized formulation of different tube theories and a semi-empirical concept of a strain-dependent finite extensibility parameter. The ABGIL equation has now been extended for filler-reinforced networks (ABGILFIL equation) by incorporating the concept of Klüppel et al. of a strain-amplification function describing the strain-induced filler-cluster breakdown. The proposed ABGILFIL equation is shown to offer a very good description of stress–strain dependences in different deformation modes of virgin and strain-softened networks of natural rubber and SBR, up to high strains. From the knowledge of the first-extension behavior, the Mullins-type strain-softening is predicted and shown to be composed of two contributions: the strain-induced filler-cluster breakdown and the strain-induced increase in the network mesh size, which is consistent with the mechanism of entanglements removal at the matrix–filler interface recently proposed and discussed by Hanson et al.

Keywords: Elastomers; Fillers; Constitutive equation

1. Introduction

A constitutive equation (free energy, strain-energy density) of an elastomeric material expresses the energy per unit volume, W, as a function of the state of strain. From W, the two principal (engineering) stresses σ_i ($i = 1,2$) (with $\sigma_3 = 0$) can be calculated:

$$\sigma_i = \frac{\partial W}{\partial \lambda_i} - \frac{\lambda_3}{\lambda_i}\frac{\partial W}{\partial \lambda_3} \tag{1}$$

λ_i ($i = 1,2,3$) are the principal stretch ratios. At constant volume, $\lambda_3 = 1/\lambda_1\lambda_2$.

Structure-based constitutive equations for homogeneous elastomeric networks, predicting both low-strain-softening and high-strain finite extensibility effects, were derived by Edwards and Vilgis [1], Kaliske and Heinrich [2] and Klüppel and Schramm [3]. A constitutive equation (ABGIL) based on the Langevin elasticity theory was proposed by the authors and subjected, with a good success, to a thorough experimental testing using biaxial stress–strain data [4,5]. All the named constitutive equations are composed of two parts, $W = W_A + W_B$, where the connectivity part W_A is due to network junctions and the constraint part, W_B is due to topological constraints. Miehe et al. [6] presented a new micro-mechanically based network model which is claimed to substantially improve the modeling capacity of the older models and examples of its ability to describe experimental data were shown.

Klüppel and Schramm extended their treatment to filler-reinforced networks [3]. They combined their non-Gaussian tube model of rubber elasticity with a damage model of strain-induced filler-cluster breakdown and arrived at a strain-dependent hydrodynamic amplification factor. With its use, Klüppel and Schramm [3], Heinrich et al. [7] and Luo et al.

* Corresponding author. Tel.: +420 296 809 384; fax: +420 296 809 410.
E-mail addresses: meissner@imc.cas.cz (B. Meissner), matejka@imc.cas.cz (L. Matějka).

0032-3861/$ - see front matter © 2006 Elsevier Ltd. All rights reserved.
doi:10.1016/j.polymer.2006.09.036

[8] were able to get a good description of virgin uniaxial stress–strain dependences of filler-reinforced elastomeric networks and of the prestrain-induced softening, commonly denoted as the Mullins effect [9,10].

The non-affine micro-sphere model of Miehe et al. [6] was extended by Göktepe and Miehe [11] to predict the behavior of filler-reinforced networks. The Mullins-type stress softening effect is considered to be due to the breakdown of chain-particle bonds. A very good description of experimental stress–strain and strain-softening data was obtained including that of the anisotropy effects and permanent set. However, although the theory is based on a molecular model, comparison of its results with experimental data affords parameter values which do not seem to be clear characteristics of the network structure. This is shortly discussed in Appendix A.

In this paper, we test the potential of the strain-dependent hydrodynamic amplification factor to give a satisfactory description of the biaxial stress–strain behavior of filler-reinforced networks. For this purpose, we use, in the first step, the Klüppel–Schramm constitutive equation [3] and, in the second step, the ABGIL constitutive equation [4,5]. The result is applied to the problem of the Mullins-type strain-softening. The experimental data are taken from published papers.

1.1. The Klüppel–Schramm model of elasticity of filler-reinforced elastomer networks

Following from the Klüppel–Schramm constitutive equation [3] the nominal (engineering) stresses σ_i ($i=1,2$) read:

$$\sigma_i = G_c\left(\frac{1-d}{(1-dI_m)^2}-\frac{d}{1-dI_m}\right)\left(\lambda_i^2-\lambda_3^2\right)/\lambda_i + 2G_e\left(\lambda_3^{-1}-\lambda_i^{-1}\right)/\lambda_i \quad (2)$$

$$I_m = I_1 - 3; \quad I_1 = \sum_{i=1}^{3}\lambda_i^2; \quad d = T_e/n_e \quad (2a)$$

I_1 is the first strain invariant, T_e the Langley trapping factor ($0 \le T_e \le 1$), n_e the number of statistical segments between two successive entanglements, G_c the elastic modulus due to network junctions (crosslinks), G_e the topological constraint modulus (proportional to the density of entanglements of the polymer). In uniaxial extension (UE), $\sigma_2 = 0$, and the stress σ_1 is calculated with $\lambda_2 = \lambda_3 = 1/\lambda_1^{1/2}$, $I_1 = \lambda_1^2 + 2/\lambda_1$. In equibiaxial extension (EBE), $\lambda_2 = \lambda_1$, $\sigma_2 = \sigma_1$, $I_1 = 2\lambda_1^2 + 1/\lambda_1^4$.

Eq. (2) applies to homogeneous (unfilled) networks. It was shown to give a very good description of uniaxial stress–strain dependences (up to high strains) obtained for a variety of crosslinker concentrations in natural rubber networks under conditions suppressing the occurrence of strain-induced crystallization [12]. It is claimed to pass the plausibility test, i.e., to represent data in different deformation modes [3].

The presence in a soft highly deformable rubbery matrix of hard and much less deformable filler particles leads to hydrodynamic effects: the required macroscopic (external) strain, ε_i, is achieved with the microscopic (internal) strain in the elastomer matrix, $\varepsilon_{i,\mathrm{int}}$, being higher than ε_i. The hydrodynamic reinforcement refers to a strain-amplification factor [3].

$$X = \varepsilon_{i,\mathrm{int}}/\varepsilon_i \quad (3)$$

$$\lambda_{i,\mathrm{int}} = 1 + \varepsilon_{i,\mathrm{int}} = 1 + X\varepsilon_i$$

The internal (microscopic) stretch ratio is assumed to be amplified to $\lambda_{i,\mathrm{int}} = 1 + X\varepsilon_i$ and this quantity should be inserted for λ_i in Eq. (2) in order to calculate the internal first strain invariant, $I_{1,\mathrm{int}}$, and the macroscopic stress observed at a macroscopic (external) strain ε_i (external stretch ratio $\lambda_i = 1 + \varepsilon_i$). The information on X is obtained from stress–strain measurements.

Filler particles are generally aggregated into clusters which, with increasing strain, may be expected to undergo breakdown and decrease in size. Two approaches to filler-cluster breakdown were considered [3,7,8]: cluster decay according to a power law and cluster decay according to an exponential law. In accordance with [8], the first approach will be considered here. The relevant strain-amplification factor becomes a decreasing function, $X(\varepsilon_i)$, of the external strain and, after a constitutive generalization is carried out [8], X is expressed as a function, $X(E)$, of a scalar strain variable E:

$$X(E) = X_\infty + (X_o - X_\infty)(1+E)^{-\alpha} \quad (4)$$

$$E = \left(\sum_{i=1}^{3}(1+\varepsilon_i)^2/3\right)^{1/2} - 1 \quad (5)$$

Limit values of X at zero and infinite strains are X_o and X_∞, respectively, while α determines the rate of decay of $X(E)$ with the strain function E. The three parameters, X_o, X_∞ and α were shown to be related to the particle size and to the structure, size, fractal dimension and anomalous diffusion coefficient of the clusters [3].

During the first stretching of a filler-reinforced network, the amplification factor decreases with strain [3,7,8] and at a maximal applied external strain, when E attains the value of $E_{\max}$, it diminishes to $X(E_{\max})$. On repeated stretching to $\varepsilon_{i,\max}$, the uniaxial stress–strain dependence becomes stabilized for strains not exceeding $\varepsilon_{i,\max}$, since the amplification factor, $X(E_{\max})$, has reached a constant value for all strains not exceeding the prestrain $\varepsilon_{i,\max}$ (i.e., for $\varepsilon_i < \varepsilon_{i,\max}$, $E < E_{\max}$).

Klüppel et al. [3,7,8] measured uniaxial stress–strain dependences of filled SBR and EPDM rubbers at various prestrains, fitted Eqs. (2)–(5) to the data and in this way determined the six parameters contained in these equations. With increasing filler concentration, the parameters G_c, G_e, X_o, X_∞ and α showed a tendency to increase. Although in the limit of infinite strain the theoretically expected minimum admissible value of X_∞ should not be lower than unity, for some systems values lower than unity or even negative were found. However, in the experimental range of the stretch ratio, the strain-amplification factor X always remained reasonably higher than the physically realistic value of unity.

Klüppel and Schramm [3] also compared the Edwards–Vilgis approach to finite network extensibility (Eq. (2)) with the classical inverse Langevin approach in the non-Gaussian tube model. Using the Padé approximation for the inverse Langevin function, they expressed the stress in uniaxial extension, σ_{UE}, in the form (Eq. (16′) in Ref. [3]):

$$\sigma_{UE} = \frac{G_c}{3}\left(\lambda\frac{3N_3-\lambda^2}{N_3-\lambda^2} - \lambda^{-2}\frac{3\lambda N_3-1}{\lambda N_3-1}\right) + 2G_e\left(\lambda^{-1/2}-\lambda^{-2}\right) \quad (2')$$

where the first term on the right-hand side can be derived from the James–Guth equation based on a three-chain network model [13]. λ is the stretch ratio in uniaxial extension, N_3 the number of statistical segments in a network chain between successive crosslinks. A combination of the inverse Langevin approach to the finite network extensibility with a constraint term based on a non-Gaussian tube model was applied by Klüppel et al. in several papers [14–17]. Klüppel and Schramm found that Eqs. (2)–(5) gave a better description of the stress–strain data on prestrained carbon black-reinforced SBR samples than Eqs. (2′)–(5) and concluded that the Edwards–Vilgis approach is to be preferred [3].

The earlier papers of Klüppel et al. [3,7,8] led to the conclusion that the pronounced strain-softening in carbon black and silica-reinforced SBR and EPDM rubbers in uniaxial extension can be quantitatively described by the non-Gaussian tube model of rubber elasticity combined with the damage model of strain-induced breakdown of filler clusters, the breakdown of filler clusters being the only mechanism determining the prestrain-softening (the Mullins effect) in filler-reinforced elastomers. In a more recent paper [18], however, Klüppel and Meier have concluded that the simple one-mechanism damage model does not give a sufficiently precise data description in uniaxial extension and, more seriously, reasonable predictions for the equibiaxial extension. They ascribed this failure to the inadequacy of the simple damage model and developed a new micro-mechanical model that assumes two mechanisms: a strain-induced breakdown of rigid filler clusters and a cyclic breakdown and re-aggregation of more fragile filler clusters. This two-mechanism model predicts prestrain-softening and filler-induced hysteresis. An improved fit to uniaxial and equibiaxial stress–strain data of filler-reinforced SBR networks is claimed [18–21].

1.2. Tests of the Klüppel–Schramm approach

James et al. prepared sulfur/accelerator crosslinked natural rubber networks both unfilled (NR gum [22]) and carbon black-reinforced (NR 40, containing 40 phr of HAF black [23]; according to a more detailed classification, the basic HAF grade is denoted as N330). They performed biaxial stress–strain measurements under carefully controlled conditions on specimens softened by prestraining to obtain repeatable stress–strain dependences. We compare these data with the predictions of the Klüppel one-mechanism damage model.

Fig. 1 shows a Mooney–Rivlin plot of the experimental results in uniaxial and equibiaxial extension, both on the unfilled and filled networks. A general definition of the reduced stress, $\sigma_{i,red}$, can be given using the stretch ratio function contained in the crosslink term of Eq. (2):

$$\sigma_{i,red} = \sigma_i / \left(\lambda_i - \frac{\lambda_3^2}{\lambda_i}\right) \quad (6)$$

For uniaxial extension (UE)

$$\lambda_2 = \lambda_3, \quad \lambda_i - \frac{\lambda_3^2}{\lambda_i} = \lambda_1 - \frac{1}{\lambda_1^2} \quad (7a)$$

for equibiaxial extension (EBE)

$$\lambda_2 = \lambda_1, \quad \lambda_i - \frac{\lambda_3^2}{\lambda_i} = \lambda_1 - \frac{1}{\lambda_1^5} \quad (7b)$$

The stress–strain data in uniaxial extension obtained on the unfilled network are described by the three-parameter Eq. (2) very well (curve 1). However, if the fitted parameter values (given in Table 1) are used to calculate the stress–strain behavior in equibiaxial extension (curve 2), then the obtained stress is obviously grossly overestimated. In other words, Eq. (2) does not pass the plausibility test, not even in the case of an unfilled network. The same conclusion was already reached in our previous paper [4] where Eq. (2) was compared with the well-known Rivlin–Saunders data [24]. We have ascribed the discrepancy to the inadequacy of the constraint term in Eq. (2).

Similar to unfilled networks, the uniaxial extension measurements on the prestrain-softened carbon black-filled NR 40 network can be described by Eqs. (2)–(5) very well (Fig. 1, curve 3). The presence of carbon black leads to an increase in G_c with only minor or zero changes in G_e and n_e/T_e (Table 1). The fitted value of the strain amplifier (1.45)

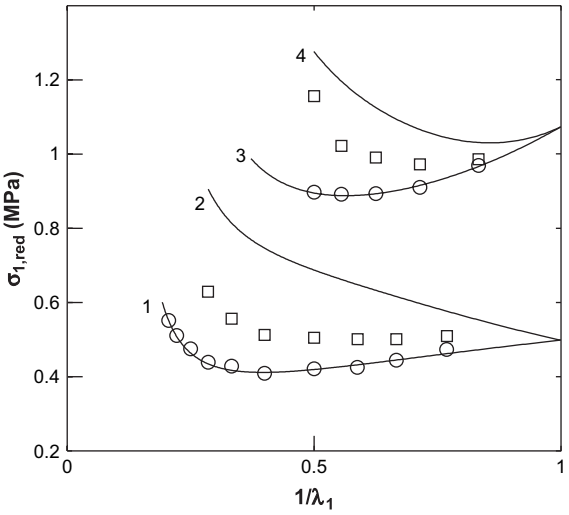

Fig. 1. Comparison of the Klüppel model [3,7,8] (curves) with uniaxial (○) and equibiaxial (□) stress–strain data on gum and filled NR networks [22,23]. Curves: NR gum, 1 – UE, 2 – EBE; NR 40, 3 – UE, 4 – EBE. Curves are drawn using parameter values given in Table 1.

Table 1
Parameters of Eqs. (2)–(5) for Fig. 1

Parameters	NR gum	NR 40
G_c (MPa)	0.310	0.573
G_e (MPa)	0.195	0.180
n_e/T_e	90	90
X		1.45

Data: NR gum [22], NR 40 [23].

is not large; it is independent of strain, as can be expected for a strain-softened network. Again, however, the equibiaxial stress prediction (curve 4) based on UE measurement is highly overestimated and the reason for this is obviously the same as in the case of the unfilled network, i.e., the inadequacy of the constraint term.

In summary, even though describing with a good success some of the uniaxial extension data, Eqs. (2)–(5) are not able to use this knowledge for a correct prediction of the equibiaxial behavior of both unfilled networks and a prestrained filler-reinforced network. The reason cannot be ascribed to an inadequacy [18] of the one-mechanism damage model.

A question arises why the plausibility test was passed with the Klüppel–Schramm data on their unfilled NR network [3] and not with the James data (Fig. 1). A comparison of the two sets of data is shown in Fig. 2, where the respective ratios R of the equibiaxial-to-uniaxial reduced stresses are plotted vs stretch ratio. Further data on two NR networks and one IR network are included in Fig. 2.

The experimental measurements of Rivlin and Saunders, Treloar, James et al. and Kawabata et al. (for references and a more detailed information on the data see Ref. [4]) are the most reliable and trustworthy of those published so far. The ratios R following from their data at the stretch ratio 1.8 have values in the range 1.2 ± 0.04. On the other hand, the Klüppel–Schramm value of R at the stretch ratio 1.8 is significantly higher (≈ 1.5); such result is improbable and casts serious doubts on the credibility of their equibiaxial measurements. The conclusion of Klüppel and Schramm that their Fig. 6 in Ref. [3] supports the developed concept of rubber elasticity (expressed by Eq. (2)) does not seem to be well-founded. Klüppel et al. [20] themselves mention possible errors in their equibiaxial measurements on filler-reinforced networks due to friction of the rolls in their stretching frame. They consider the necessity of further biaxial investigations using the bubble inflation test.

Further question concerns the general applicability of the Edwards–Vilgis approach to the finite network extensibility. Eqs. (2)–(5) are claimed to give – contrary to the inverse Langevin approach – a good description of the upturn behavior in the stress–strain dependence of a prestrained filler-reinforced network [3]. One can conjecture that Eq. (2) should then be able to describe the upturn behavior of prestrained *unfilled* networks. An example of stress–strain data on a prestrained lightly crosslinked network SBR B is shown in Fig. 3. Data are taken from Ref. [25]; the effect, on the stretch ratio, of tension set existing at the beginning of the second extension was eliminated by subtracting a strain-dependent correction. For the initial, i.e., the highest zero-stress stretch ratio, λ_s, the correction is equal to $(\lambda_s - 1)$, thus giving the corrected stretch ratio $\lambda_{cor} = 1$. For the highest stretch ratio on second extension, λ_m (equal to that on first extension), the correction is assumed to be zero and $\lambda_{cor} = \lambda_m$. For intermediate stretch ratios, λ (the index 1 is dropped), the magnitude of correction was assumed to decrease linearly from $(\lambda_s - 1)$ to zero: $\lambda_{cor} = 1 + (\lambda_m - 1)(\lambda - \lambda_s)/(\lambda_m - \lambda_s)$. The curve in Fig. 3 which is fitted to experimental points using Eq. (2) is able to represent only a part of the data. The upturn of experimental stress at high strains is more rapid than predicted by the Edwards–Vilgis approach and, in contrast to the behavior of prestrained filler-reinforced networks, no successful data representation can be obtained.

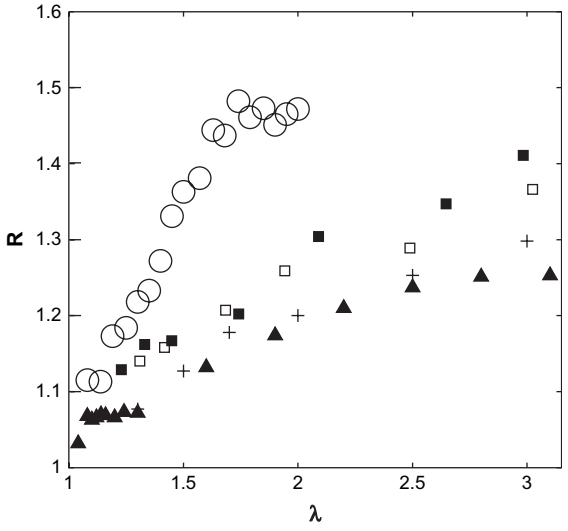

Fig. 2. Dependence of the ratio, R, of the equibiaxial-to-uniaxial reduced stress on stretch ratio for NR and IR networks (the index 1 in λ_1 has been dropped). R at $\lambda = 1.8$: Rivlin–Saunders ■ 1.23; Treloar □ 1.22; James et al. + 1.18; IR Kawabata et al. IR ▲ 1.16 (for references see Ref. [14]); Klüppel et al. ○ 1.48.

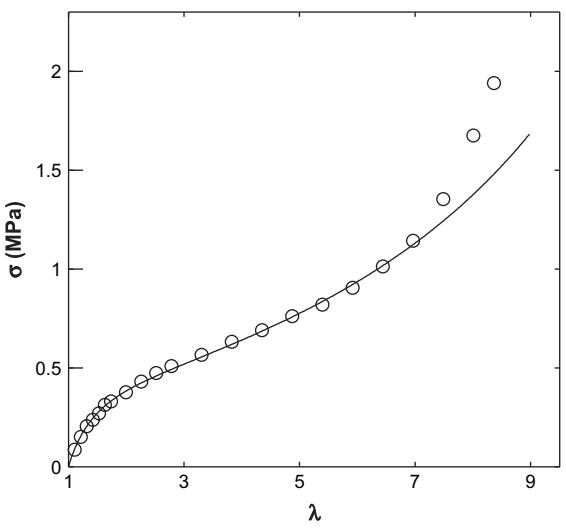

Fig. 3. Stress–stretch ratio dependence of a lightly crosslinked SBR B network on second extension, points. Curve is drawn according to Eq. (2), $G_c = 0.108$ MPa, $G_e = 0.211$ MPa, $n_e/T_e = 370$. (The index 1 in σ_1, λ_1 has been dropped.)

A similar type of behavior is observed with a virgin stress–strain dependence of an SBR network reinforced with graphitized HAF black. Data from a review of Kraus were quoted in our previous paper [26] and are plotted in Fig. 4. Eqs. (2)–(5) are fitted to experimental points using parameter values $G_c = 0.260$ MPa, $G_e = 0.800$ MPa, $X_o = 1.25$, $X_\infty = 1.0$, $\alpha = 1.0$, $n_e/T_e = 216$. The degree of clustering of graphitized black and its change with strain can be expected to be small which is reflected in a low value of the amplification factor. The data description is very good up to the stretch ratio of approx. 6.2 but thereafter the upturn of experimental stress is much more rapid than predicted by the extrapolated Klüppel–Schramm curve. Thus, in the case of a simple unprestrained polymer–filler system with a small degree of clustering, the Edwards–Vilgis approach to the finite network extensibility fails.

The examples shown in Figs. 3 and 4 strongly suggest that the crosslinking (connectivity) term of Eq. (2) does not give a suitable and universally applicable tool for the description and interpretation of the upturn behavior of the experimental stress–strain dependences. Moreover, the Edwards–Vilgis [1], Kaliske–Heinrich [2] and Klüppel–Schramm [3] treatments of the finite extensibility problem leave some open questions; these are discussed in Appendix D.

2. The ABGILpd equation and its comparison with experimental data

In previous two communications we analyzed published biaxial stress–strain data obtained on networks of natural, isoprene, styrene–butadiene and siloxane rubbers [4,5]. A critical examination of the published constitutive equations [1–3] led to the conclusion that their connectivity terms are not molecularly based. We proposed and tested a new strain-energy function denoted by the ABGI code. Its connectivity (network junction) term, W_A, is equal to the result of the Langevin elasticity theory of Arruda and Boyce (AB) [27]. The constraint term, W_B, is based on tube theories [2,3,28–33] and is expressed in a generalized phenomenological form [33] (GI, generalized invariant). The nominal (engineering) stresses σ_i ($i = 1,2$) following from the ABGI constitutive equation read:

$$\sigma_i = 2C_1 \frac{\lambda_{cm}}{3\lambda_c} L^{-1}\left(\frac{\lambda_c}{\lambda_{cm}}\right)\left(\lambda_i^2 - \lambda_3^2\right)/\lambda_i + 2C_2 \frac{2}{n}\left(\lambda_i^n - \lambda_3^n\right)/\lambda_i \quad (8)$$

$$\lambda_c = (I_1/3)^{1/2}; \quad \lambda_{cm} = N^{1/2} \quad (8a)$$

The ABGI stress–strain relations in uniaxial extension, equibiaxial extension and in pure shear are given in Appendix B.

The first term on the right-hand side of Eq. (8) follows from the Arruda and Boyce theory [27]. The symbol for the theoretical shear modulus given there as $G_{th} = \nu RT$ (ν is the network chain density) is replaced with $2C_1$, λ_c is the network chain stretch ratio, i.e., the ratio of the deformed and undeformed chain end-to-end distances, I_1 is the first strain invariant defined in Eq. (2a), λ_{cm} is the hypothetical highest possible network chain stretch ratio (or the finite extensibility parameter, locking chain stretch ratio), which is predicted to be equal to the square root of the network chain length expressed as the number, N, of statistical segments in the network chain (Eq. (8a)). The modulus component $2C_1$ contains contributions from both chemical crosslinks and trapped entanglements of a 'stable', i.e. junction-like nature; the network chain length, N, is also determined by network junctions of both types [4].

The Langevin function is defined by $L(x) = \coth(x) - 1/x$; $L^{-1}(x)$ is the inverse Langevin function which can be expressed with a satisfactory accuracy by the Padé approximation introduced by Cohen [34] (Appendix C):

$$L^{-1}(x) \approx L_{pd}^{-1}(x) = \frac{3x - x^3}{1 - x^2} \quad (9)$$

Thus, the ABGI equation can also be applied in a form which we denote by the ABGIpd code and which is simpler in calculations:

$$\sigma_i = 2C_1 \frac{1 - (\lambda_c/\lambda_{cm})^2/3}{1 - (\lambda_c/\lambda_{cm})^2}\left(\lambda_i^2 - \lambda_3^2\right)/\lambda_i + 2C_2 \frac{2}{n}\left(\lambda_i^n - \lambda_3^n\right)/\lambda_i \quad (10)$$

The second term on the right-hand side of Eqs. (8) and (10) is a phenomenological formulation [33] of the results following from different theories of the constraint effect [2,3,28–33]. It should be noted that the constraint part of the Klüppel–Schramm Eq. (2) is its special case with $n = -1$. The connectivity part of the Klüppel–Schramm Eq. (2′) is based on the three-chain network model of James and Guth [13] whereas the connectivity part of the ABGIpd Eq. (10) is based on the eight-chain network model of Arruda and Boyce; for uniaxial extension and $N_3 \approx 3N$, the two models predict practically the same dependences [25].

The constraint contribution to the modulus, often denoted as G_e in tube theories and replaced here with $2C_2$, is proportional to d_o^{-2}, where d_o is the tube radius (mean fluctuation radius of the segment) in the undeformed state [2]. The tube radius is

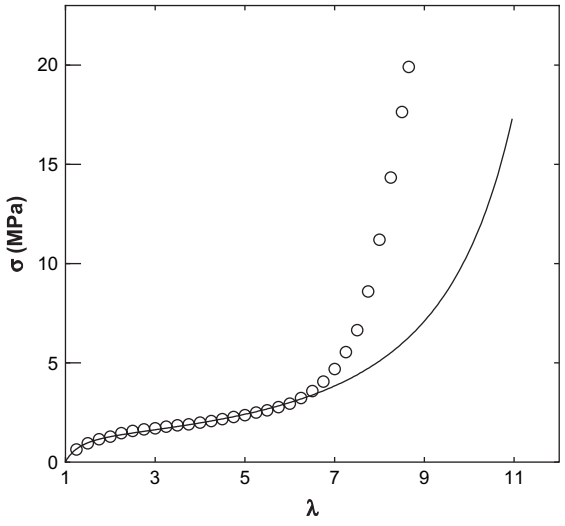

Fig. 4. Points: experimental data of Kraus on an SBR network containing graphitized HAF black. Curve is drawn according to Eqs. (2)–(5). The index 1 in σ_1, λ_1 is dropped.

assumed to scale with the mean spacing of successive chain entanglements. In the Kaliske and Heinrich treatment [2], G_e is proportional to the apparent concentration of elastically effective physical crosslinks (entanglements) arising from conformational constraints. The parameter n reflects the constraint mechanism considered in different theories and values ranging from -1 to $+1$ have been predicted [2,3,28–33]. Gaylord and Douglas [29] admit the possibility that n is not universal for all the network structures and we have followed their suggestion to treat it as an empirical parameter.

The ABGIpd equation contains four adjustable parameters: C_1, C_2, λ_{cm}, n. The predicted low-strain behavior is essentially determined by the elastic constants C_1, C_2 and the exponent n. The high-strain behavior is increasingly governed by N which determines the square of the locking chain stretch, Eq. (8a), and hereby the maximum possible macroscopic stretch ratios which follow from the relation (8a): $I_{1,max} = 3N$. With $n = -2$ and a very large N, the ABGIpd equation reduces to the Mooney–Rivlin equation [35,36]. With $n = +2$, the stretch ratio function in the constraint term becomes identical with the prediction of the Gaussian elasticity theory.

As shown previously for natural and isoprene rubber networks [4], the ABGI($n = -2$, λ_{cm}) equation gives an excellent representation of stress–elongation data up to medium strains, slightly above the inflection point of the curve. However, for a satisfactory simultaneous description of stress–strain data in all geometrical modes, the value of n had to be increased from -2 into the region from ca -0.2 to $+1$, depending on the network. The increase in n is accompanied by a small impairment in the data description at very low strains and an appropriate compromise giving a minimum of systematic point-curve deviations in the strain dependence of the reduced stress must be found. The effect of the variation in n on the quality of data description is shown, e.g., in Figs. 6–12 and Tables 3–5 in Ref. [4]; an optimal value of n was usually determined with an accuracy of approx. ± 0.2.

The virgin stress–strain dependences at high strains are in a majority of cases more complex in all geometrical modes than expected by the ABGI equation [4]. On the other hand, prestrained networks tend to show a simpler behavior than the unprestrained ones [25,26,37]. In Fig. 5 we compare the ABGIpd Eq. (10) (curve 2) with the data (open circles) obtained on second extension of an unfilled lightly crosslinked SBR B network (data already shown in Fig. 3). The fit of the curve 2 to the data in Fig. 5 is very good in the whole stretch ratio range and the upturn behavior of the prestrained network is represented by the ABGIpd inverse Langevin approach with a very good success, in contrast to the failure of the Edwards–Vilgis approach shown in Fig. 3.

The stress–strain dependence obtained on the *first* extension can be described by the ABGIpd curve 1a ($\lambda_{cm} = 4.743$) up to the stretch ratio $\lambda \approx 5.5$, slightly above the inflection point of the experimental dependence. Thereafter the experimental stress increases with a smaller slope than expected by curve 1a. This observation was interpreted in our previous paper [25] as a relaxation effect which may be ascribed to some kind of strain-induced reorganisation of the network

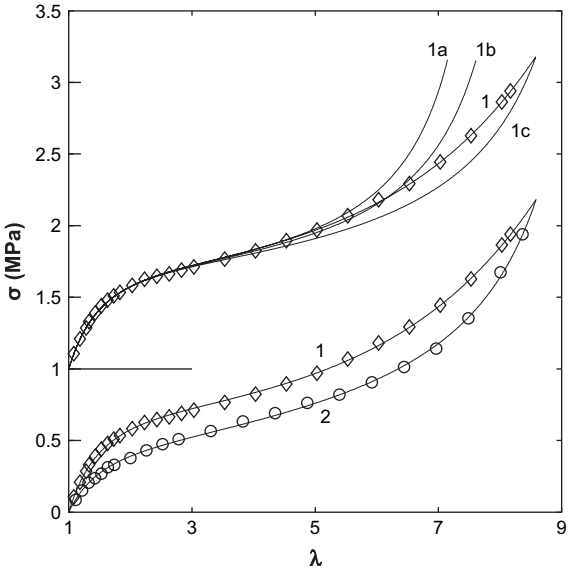

Fig. 5. Stress–stretch ratio dependences of network SBR B. Points, experimental; ○ – first extension, ◇ – second extension. Curves 1a, 1b, 1c, 2 are drawn according to the ABGIpd equation, curve 1 according to the ABGILpd equation. The index 1 in σ_1, λ_1 is dropped.

topology, its extent increasing with increasing stretch ratio. If so, then at high strains the parameters of the ABGI equation should become functions of strain: the extensibility parameter will increase, modulus components decrease with strain. Microscopically this could mean that some independent circuitous paths are disappearing from the network while the average size of the circuitous paths increases. A possible mechanism can be imagined. Trapped entanglements contributing to C_1 – in spite of behaving as stable network junctions at low and medium strains – may be forced by the increasing stress to slip along the network chains (cf. [1]), in principle up to the nearest crosslinks. This would modify the network topology and lead to an increase in the network mesh size which would partially persist on retraction and on second and subsequent extensions. High-extension hysteresis, time-dependent tension set and anisotropy can be envisaged as possible consequences. Permanent flow might be a contributing factor in very lightly crosslinked networks. In the undeformed state, a partial (or complete) recovery of the original topology can be expected to take place.

Since at high strains the stress is dominated by the extensibility parameter, we have assumed that the modulus components can be treated in the first approximation as independent of strain. Information on the strain dependence of the extensibility parameter is obtained by comparing the experimental dependence with the ABGI equation, as described in more detail in Ref. [4]. In Fig. 5 one can see that curve 1b, with a somewhat higher $\lambda_{cm} = 5.1$ than used for curve 1a, intersects the experimental dependence at $\lambda \approx 6.0$ while the curve 1c with $\lambda_{cm} = 5.865$ intersects it at the stretch ratio $\lambda \approx 8.6$. From a more detailed information of this kind it is possible to obtain the dependence of λ_{cm} on λ and, using Eq. (8a), on λ_c.

The concept of a strain-induced increase in the finite extensibility parameter was utilized by us for the first time for the description of tensile stress–strain dependences [25,26,37]

and subsequently generalized under the designation of the ABGIL equation for the description of biaxial stress–strain data, as discussed in more detail earlier [4,5]. The letter 'L' in the ABGIL code is added to indicate that in this case the finite extensibility parameter is considered to be a function of stretch ratios, λ_i. The possibility of a strain-induced increase in the network mesh size at high strains was anticipated in the literature (Wu and van der Giessen [38], cf. [4]) but no theoretical treatment of the effect was proposed. The dependences of λ_{cm} on λ_c obtained from experimental data can generally be described by a phenomenological function of a simple form:

$$\lambda_c \le \lambda_{c,a}, \quad \lambda_{cm} = \lambda_{cm,a}$$

$$\lambda_c > \lambda_{c,a}, \quad \lambda_{cm} = \lambda_{cm,a} + (\lambda_{cm,b} - \lambda_{cm,a})[(\lambda_c - \lambda_{c,a})/(\lambda_{c,b} - \lambda_{c,a})]^a \tag{11}$$

Hence, the ABGIL equation is given by Eqs. (8) and (11) and the ABGILpd equation is given by Eqs. (10) and (11). For chain stretch ratios lower than $\lambda_{c,a}$, the finite extensibility parameter is constant and equal to $\lambda_{cm,a}$. For chain stretch ratios higher than $\lambda_{c,a}$, attained not far above the inflection point of the stress–strain curve, the finite extensibility parameter begins to increase with strain and at the chain stretch ratio $\lambda_{c,b}$ it attains the value $\lambda_{cm,b}$. The chain stretch ratio $\lambda_{c,b}$ is given by the highest stretch ratio used in the experiment; sometimes the sample is stretched up to the break. Thus, $\lambda_{c,b}$ is not an adjustable parameter and $\lambda_{cm,b}$ has a very limited freedom of adjustment. The five parameters in Eq. (11), only three of them being fully adjustable parameters, describe the range and extent of the increase in λ_{cm} and determine the stress–strain behavior above the inflection point while being of much less importance for the low-strain behavior. Tests of the fitting procedure do not reveal any signs of instability.

The ability of the ABGILpd curve 1 to describe the virgin stress–strain dependence of the SBR B network is shown in Fig. 5; parameters are given in Table 2. The extensibility parameter increases from 4.74_3 to 5.86_5 and, as anticipated, the second value determines then the high-strain behavior of the network on second extension. The prestrain had little effect on the connectivity part of the modulus, $2C_1$, while the constraint modulus, $2C_2$, decreased. In the lower part of Fig. 5, the stress–strain dependences obtained on the first and second extension are depicted together. The hysteresis loop resulting from strain-softening resembles that of filler-reinforced networks. Due to prestrain, the strain energy of the given network sample has decreased by 20%.

Table 2
Parameters of the ABGIpd and ABGILpd equations for curves in Fig. 5, network SBR B; $n = 0.2$

Parameter	Curves				
	1a	1b	1c	1	2
C_1 (MPa)	0.042	0.042	0.042	0.042	0.0455
C_2 (MPa)	0.195	0.195	0.195	0.195	0.1045
λ_{cm}	4.74_3	5.10	5.86_5		5.86_5
$\lambda_{c,a}$				2.34_5	
$\lambda_{cm,a}$				4.74_3	
$\lambda_{c,b}$				4.96_7	
$\lambda_{cm,b}$				5.86_5	
a				1.50	

The ABGIL equation was previously compared with biaxial stress–strain measurements on natural rubber networks differing in the degree of crosslinking [4]. The C_1, λ_{cm}, parameters reflect the changes in the degree of crosslinking, as expected. The values of the parameter n were found to range from -0.2 to $+1$ [4,5]. This corresponds to the predictions of four different theoretical treatments [3,28–33] without giving an unequivocal support to any of them. The ABGIL equation was shown to provide a good basis for a quantitative interpretation of tensile properties of double network rubbers [39] up to high stretch ratios.

The detailed biaxial stress–strain measurements of James et al. on an NR gum network [22] and on a corresponding NR filler-reinforced network prepared under conditions giving essentially the same matrix structure [23] offer a unique opportunity to get information on the effect of filler. To get a picture as complete as possible, the previously performed testing of the ABGIL equation using data on the gum network of James et al. [4] is supplemented here by further data – equation comparisons.

An excellent ability of the ABGILpd Eqs. (10) and (11) to represent the general biaxial stress–strain data on an NR gum network [22] is shown in Fig. 6 in the plot of $\log \sigma_1$ vs λ_2 for different constant values of λ_1 and in Fig. 7 in the plot of reduced stresses vs reciprocal stretch ratio (curves 1, 1a, 2, 2a). The fitted parameter values are given in Table 3. Fig. 6 shows that the *relative* point-curve deviations are fairly small; most of them do not exceed 5%. Reduced stresses (Fig. 7) also reflect relative deviations of experimental points from the fitted curves in a sensitive manner. In Fig. 7, all available data in uniaxial extension (up to $\lambda_1 = 4.8$) have been plotted.

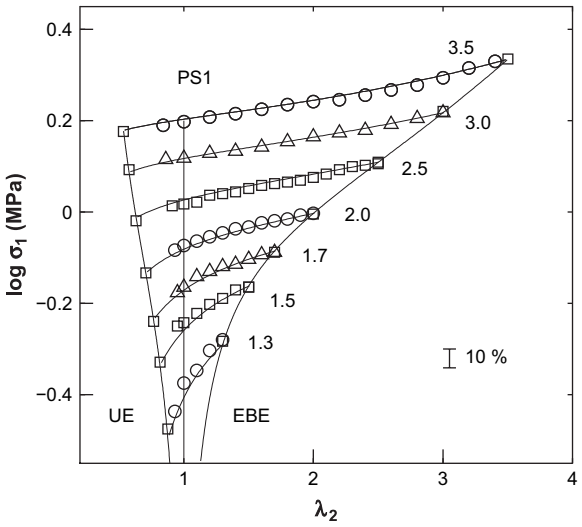

Fig. 6. Dependence of $\log \sigma_1$ (MPa) on λ_2 at constant values of λ_1 (indicated in the graph). Points: NR gum [22]. Curves: Eqs. (10) and (11), parameters are in Table 3.

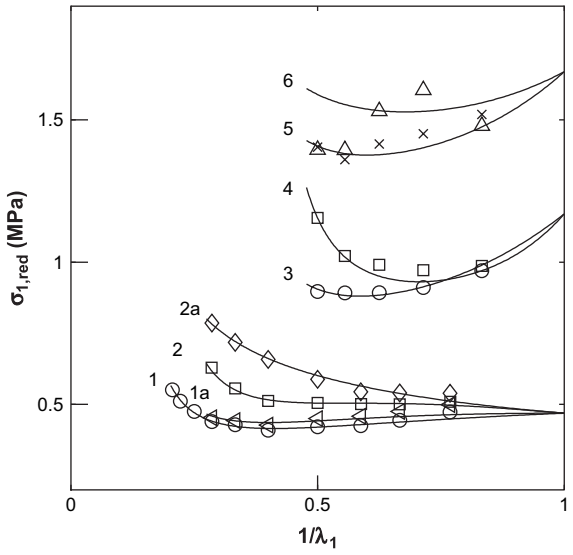

Fig. 7. Dependence of reduced stresses on reciprocal stretch ratio. Points: data [22,23]. Curves: Eqs. (10), (11), (3)–(5), parameters are in Table 3. NR gum: 1 – UE ○, 1a – PS1 △, 2 – EBE □, 2a – PS2 ◇. NR 40: 3 – UE ○, 4 – EBE □, 5 – PS1 ×, 6 – PS2 △. Curves 5, 6 and the corresponding PS points are shifted vertically by +0.5 MPa.

3. The ABGILFILpd equation and its experimental testing

Following the approach of Klüppel and Schramm [3] described in Section 1.1, we have applied the ABGILpd equations (10) and (11) together with Eqs. (3)–(5) to process the data of James and Green [23] on prestrained specimens of the natural rubber network NR 40 containing 40 phr of HAF carbon black. The combination of Eqs. (10), (11), (3)–(5), which we denote as ABGILFILpd, was fitted to the experimental data and the result is shown in Figs. 7 and 8. The obtained parameter values are given in Table 3. An appropriate value of the exponent n lies around 0.2 as before for the gum network. The addition of carbon black leads to an increase in the modulus components C_1, C_2 and the finite extensibility parameter of the prestrain-stabilized filled network is independent of deformation, in accordance with our previous findings [37]. Also, the amplification factor is independent of deformation, in accordance with the measurements of Klüppel et al. [3,7,8]. Thus, five parameters are sufficient to represent the behavior of prestrained specimens in uniaxial and equibiaxial extensions with a very good accuracy, and the behavior in pure shear with a satisfactory accuracy. The transverse shear stresses at the highest strains seem to suffer from experimental scatter. Also, the biaxial stresses obtained around $\lambda_1/\lambda_2 = 1.8/1.5$ and 2.0/1.6 are seen in Fig. 8 to deviate towards lower values more than suggested by neighboring data. Nevertheless, for a molecularly based theory, the overall measure of agreement between the data and fitted curves, which is seen both in Fig. 7 and in Fig. 8, can be denoted as satisfactory. Only very few points deviate by as much as 8–10%.

Table 3
Parameters of the ABGILpd and ABGILFILpd equations for four NR networks (curves in Figs. 6–9); $n = 0.2$

Parameter	NR gum	NR 40 prestrained	NR 23 virgin	NR 69 virgin
C_1 (MPa)	0.145	0.195	0.125	0.135
C_2 (MPa)	0.081	0.100	0.070	0.175
λ_{cm} [a]		3.36		
X [b]		1.90		
$\lambda_{c,a}$	1.69		1.60	1.90
$\lambda_{cm,a}$	3.52		3.38	3.55
$\lambda_{c,b}$	2.86		2.11	3.59
$\lambda_{cm,b}$	3.85		3.60	4.64
a	1.50		1.12	1.12
X_o			2.6	5.9
X_∞			0.22	0.22
α			0.40	0.65
λ_m (UE)	4.8	2.0	2.10	2.03
λ_{min}	2.5	1.72	1.75	1.5
$\Delta\sigma_{red}$ (%)	11.7	18.7	34.6	54.6
σ_{red} ($\lambda = 1$) (MPa)	0.47	1.17	1.05	3.7

λ_m (UE) – the highest stretch ratio used in uniaxial extension; λ_{min} – stretch ratio at the minimum reduced UE stress; $\Delta\sigma_{red}$ – the percent decrease in reduced UE stress from $\lambda = 1$ to $\lambda = \lambda_{min}$; σ_{red} ($\lambda = 1$) – reduced UE stress at zero strain.

[a] Extensibility parameter independent of strain.

[b] Strain amplifier independent of strain.

The ability of the ABGILFILpd equation to describe the uniaxial and equibiaxial stress–strain data of Davies et al. [40] on unprestrained NR networks containing 23 phr (NR 23) and 69 phr (NR 69) carbon black of the HAF (N330) grade is shown in Fig. 9. Davies et al. found that data on carbon black-filled NR networks obtained in different deformation modes (uniaxial extension, uniaxial compression, simple and pure shear) superimposed quite closely when plotted in the log–log coordinates of the reduced stress vs ($I_1 - 3$). In Fig. 9, only data in uniaxial extension and uniaxial compression are plotted; data in shear lie between them. It should be recalled that uniaxial compression along one direction (say, direction 3, with stretch ratio $\lambda_3 < 1$) produces the same state of strain as equibiaxial extension in the other two directions ($\lambda_1 = \lambda_2 > 1$) providing that

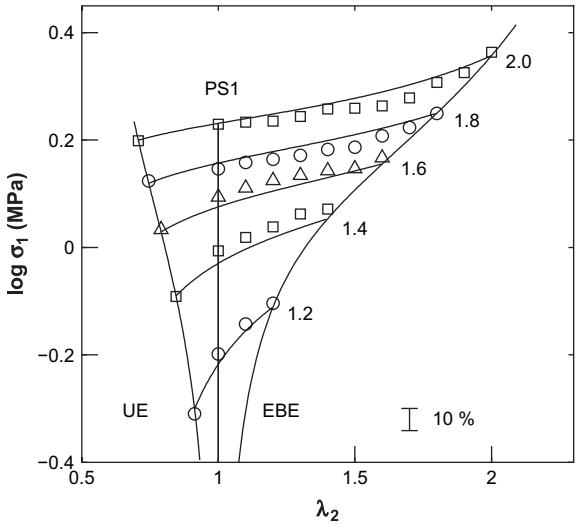

Fig. 8. Dependence of log σ_1 (MPa) on λ_2 at constant values of λ_1 (indicated in the graph). Points: NR 40 [23]. Curves: Eqs. (10), (11), (3)–(5), parameters are given in Table 3.

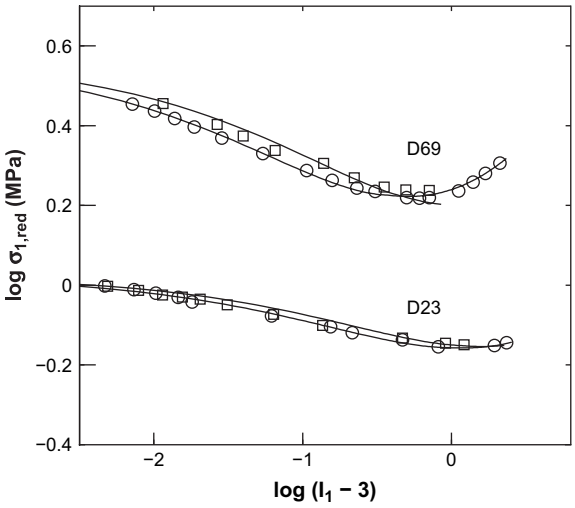

Fig. 9. Comparison of the ABGILFILpd equation (curves) with experimental data on virgin networks NR 23 and NR 69 [40]. Points: ○ uniaxial extension, □ uniaxial compression (equibiaxial extension). Curves: Eqs. (10), (11), (3)–(5), parameters are given in Table 3.

$\lambda_3 = 1/\lambda_1^2$. Under such condition, the values of $(I_1 - 3)$ in uniaxial compression and equibiaxial extension are equal and the same applies to the respective reduced stresses. The experimental dependences can be described by the theoretical curves very well. Only two points show a somewhat higher deviation (between 5 and 10%) while all other points deviate less than 4%. The amplification factor (see Table 3) decreases with strain, in accordance with the findings of Klüppel and Schramm [3], and the finite extensibility parameter increases with strain in conformity with our previous results [37]. The optimum value of the exponent n in the constraint term was found to be 0.2, i.e. it is significantly higher than the value of −1 following from the Klüppel–Schramm model [3].

In Fig. 10, the Kraus data on an SBR network containing graphitized HAF black (data already shown in Fig. 4) are

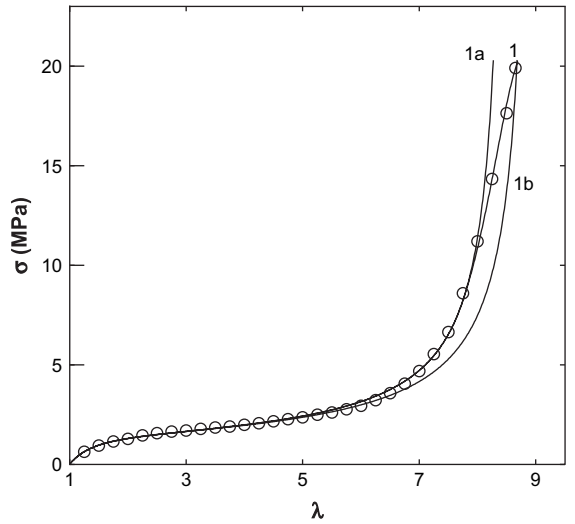

Fig. 10. Points: experimental data of Kraus on an SBR network containing graphitized HAF black, first stretching. Curves: ABGILFILpd, Eqs. (10), (11), (4), 1a – $\lambda_{cm} = 5.52$; 1b – $\lambda_{cm} = 5.80$; 1 – λ_{cm} increasing from 5.52 to 5.80. The index 1 in σ_1, λ_1 is dropped.

compared with the ABGILFILpd equation. The obtained parameter values are given in Table 4. Curve 1a with a constant finite extensibility parameter $\lambda_{cm} = 5.52$ is able to give an excellent representation of the experimental data up to 90% of the strain at break and up to two thirds of the stress at break. In the region of the highest strain, the experimental stress increases less rapidly than curve 1a. This is ascribed to a gradual strain-induced increase in λ_{cm} up to 5.8, the value which is used for curve 1b. The decrease in X with strain is small (from 1.25 at zero strain down to 1.126 at the highest stretch ratio 8.64) and the predicted strain-softening due to filler-cluster breakdown is thus practically zero. The finite extensibility parameter shows a less significant increase with strain than it does in networks containing non-graphitized blacks. Nevertheless, some softening is predicted to take place. Curve 1b can serve as an estimate of the stress–strain dependence on second extension.

4. The Mullins-type strain-softening

The ABGILFILpd equation incorporates the concepts of a strain-induced filler-cluster breakdown (Eqs. (3)–(5)) and of a strain-induced increase in the finite extensibility parameter. The first effect seems to be semipermanent; a recovery of the second one after a long time and at an increased temperature seems plausible. Provided that the time interval between the end of the first (uniaxial) extension–retraction cycle and the beginning of the subsequent second extension is not excessively long and that the temperature did not increase, both effects should contribute to prestrain-softening [9,10], commonly called the Mullins effect. This expectation is tested here in Figs. 11 and 12 using published experimental data. In the following, the index 1 in σ_1, λ_1 has been dropped.

Bueche [41] performed his stress – extension–retraction measurements under quasi-equilibrium conditions, i.e., using very low-strain rates. The recovery of the specimen length after the first extension–retraction cycle was not complete; the permanent set was, as a rule, around 10%. By swelling the specimen in benzene and subsequent evaporation of the solvent, this permanent set could be essentially removed. An

Table 4
Parameters of the ABGILFILpd equation for curves in Fig. 10; $n = 0.2$

Parameter	Curves		
	1a	1	1b
C_1 (MPa)	0.110	0.110	0.110
C_2 (MPa)	0.370	0.370	0.370
λ_{cm} [a]	5.52		5.80
X [b]			1.126
$\lambda_{c,a}$		5.0	
$\lambda_{cm,a}$		5.52	
$\lambda_{c,b}$		5.57	
$\lambda_{cm,b}$		5.80	
a		1.5	
X_o	1.25	1.25	
X_∞	1.05	1.05	
α	0.6	0.6	

[a] Extensibility parameter independent of strain.
[b] Strain amplifier independent of strain.

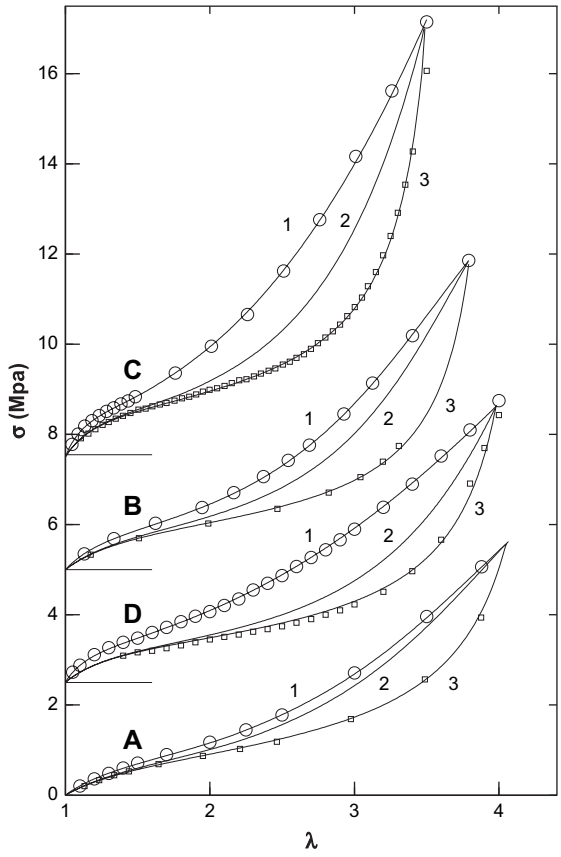

Fig. 11. Comparison of the ABGILFILpd equation (curves; parameters in Table 5) with experimental data (points: ○ first extension, □ second extension). Network A: NR 20 [42]; B: SBR 30 [41], shifted vertically by +5 MPa; C: SBR 40 [43], shifted vertically by +7.5 MPa; D: SBR 50 [9], shifted vertically by 2.5 MPa. Curves 1: first extension, X and λ_{cm} strain-dependent. Curves 2: X constant, equal to its value at maximum prestrain. Curves 3: second extension, both X and λ_{cm} constant, equal to their respective values at maximum prestrain.

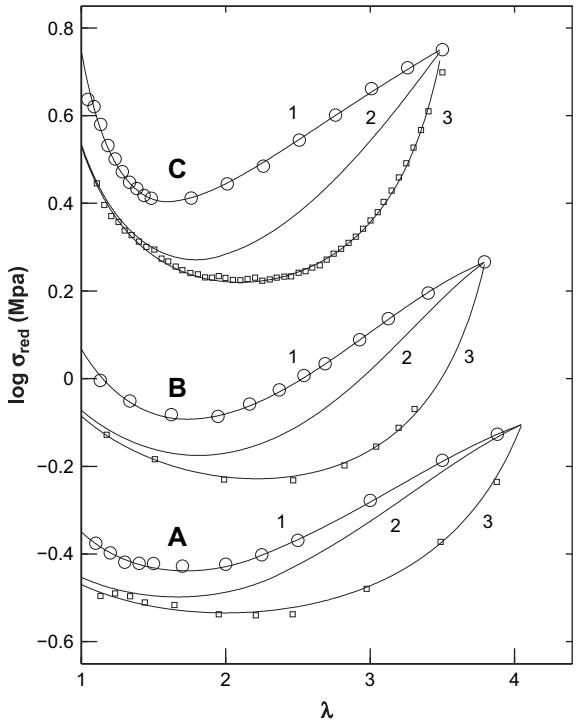

Fig. 12. Points and curves of Fig. 11 in the coordinates of log reduced stress vs stretch ratio. Curves and points A are shifted vertically by −0.25, curves and points C by +0.3.

example of measurements on an SBR 30 network (designation B in the graph) containing 30 phr of carbon black N330 is shown in linear coordinates in Fig. 11 and in the coordinates of logarithm of reduced stress vs stretch ratio in Fig. 12. The highest stretch ratio on the first extension was $\lambda_m = 3.8$. The stress at this stretch ratio is not given in Bueche's Fig. 3 [41]; we have estimated it by extrapolation. The parameter values for the first extension were then determined by fitting the ABGILFILpd equation to the data (see Table 5) and used for drawing the curves 1B in Figs. 11 and 12. The strain-amplification factor at zero strain is $X_o = 1.84$ and at the maximum prestrain ($\lambda_m = 3.8$) it drops to $X_m = 1.33_5$. Following Klüppel and Schramm [3], we assume that the strain amplifier on the second extension is equal to X_m up to the stretch ratio λ_m. However, curves 2B which are drawn using $X = X_m$, i.e., with the assumption that the filler-cluster breakdown alone is responsible for the Mullins softening, are far from giving an at least approximate description of the second-extension points. This result indicates that contrary to the conclusions of Klüppel et al., the filler-cluster breakdown is responsible for only a part of the total Mullins softening.

The fitted finite extensibility parameter on the first extension (Table 5) starts at low strains with a rather low value of 2.25 and increases up to $\lambda_{cm,m} \equiv \lambda_{cm,b} = 2.95_2$ at $\lambda_m = 3.8$. In our previous papers, a strain-induced increase in the finite extensibility parameter, or, in molecular terms, an increase in the average network mesh size, was observed and assumed to get contributions from both the matrix (sliding of entanglements) and the matrix–filler interface (sliding of filler–matrix contacts) [37]. In accordance with arguments given in our previous papers [26,37] and with the behavior of the unfilled network SBR B (Fig. 5, Table 2), we can assume that during the second extension the finite extensibility parameter is much less strain-dependent or even constant and equal to $\lambda_{cm,m}$ attained at the highest prestrain. Thus, curves 3B in Figs. 11 and 12 are drawn with $X = X_m$ and $\lambda_{cm} = \lambda_{cm,m}$. As can be seen both in the linear graph of Fig. 11 and in the highly scatter-sensitive plot of Fig. 12, the fit of curves 3B to the experimental second-extension data is convincingly good.

Another test was performed here using experimental data of Kilian et al. [43] on an SBR 40 network (C in graphs) containing a somewhat higher concentration, 40 phr, of N330 black. The effect of permanent set ($\approx 10\%$; $\lambda_s \approx 1.1$) existing at the beginning of the second extension was removed by subtracting a strain-dependent correction, in the manner described in more detail in Section 1.2. Curves 1 and 3 which are drawn using the fitted parameter values given in Table 5 describe the experimental data both on the first and second extensions very well, without any systematic deviations.

Data on an NR 20 network [33] containing a rather low HAF (N330) black concentration of 20 phr are plotted in Figs. 11 and 12 and are denoted as A. Stretch ratios on the second extension are corrected in the manner described above. To

Table 5
Parameters of the ABGILFILpd equation for networks A–D and curves in Figs. 11 and 12; $n = 0.2$

Parameter	A NR 20		B SBR 30		C SBR 40		D SBR 50	
Curves	1	3	1	3	1	3	1	3
C_1 (MPa)	0.151	0.151	0.125	0.125	0.120	0.120	0.110	0.110
C_2 (MPa)	0.096	0.096	0.172	0.172	0.210	0.210	0.146	0.146
λ_{cm}		2.92_7		2.95_2		4.57_5		3.97_3
X		1.15_8		1.33_5		2.54_2		1.71_9
$\lambda_{c,a}$	1.60		1.40		2.06		1.55	
$\lambda_{cm,a}$	2.30		2.25		3.29		3.13	
$\lambda_{c,b}$	2.64_4		2.76		4.25_6		3.66_4	
$\lambda_{cm,b}$	2.92_7		2.95_2		4.57_5		3.97_3	
a	1.50		1.73		1.37		1.95	
X_o	1.47		1.84		4.15		3.59	
X_∞	1.00		0		0.20		0.40	
α	1.26		0.40		0.72		0.95	
λ_m	4.05	4.05	3.80	3.80	3.50	3.50	4.00	4.00
$E_{r,Mull}$ (%)	27.5		35.4		40.2		38.6	
$E_{r,fill}$ (%)	26.2		38.0		53.5		69.6	
λ_{min}	1.75		1.75		1.60		1.77	
$\Delta\sigma_{red}$ (%)	18.5		30.4		53.3		51.3	
σ_{red} ($\lambda = 1$) (MPa)	0.80		1.17		2.77		1.75	

$E_{r,Mull}$ – percent of the deformation energy lost in the Mullins softening; $E_{r,fill}$ – percent of the contribution of filler-cluster breakdown to the energy lost in the Mullins softening. λ_m, λ_{min}, $\Delta\sigma_{red}$, σ_{red} ($\lambda = 1$) – see Table 3.

optimize the fit, a somewhat higher λ_m (4.05) was used in the calculation than was the experimental prestrain ratio (3.9). The quality of data representation using the fitted parameter values (Table 5) is very good.

Data of Mullins and Tobin [9] on an SBR network containing 50 phr of carbon black of the MPC type (medium processing channel black, no longer used) are shown in Fig. 11D. The description of the virgin stress–strain curve is excellent; the data on the second extension show a slight systematic downward shift in the region of medium strains but the discrepancy is not serious. A slight decrease in the C_2-parameter (of 15%) makes the fit satisfactory.

The reduced stress in uniaxial extension of virgin specimens decreases with strain to a minimum (Fig. 12) at the stretch ratio λ_{min}. For unfilled networks, λ_{min} tends to be higher than 2.0, see e.g. Fig. 1. For the carbon black-filled networks, the minimum is attained at λ_{min} lower than 2 and, with increasing carbon black content, it decreases down to 1.5 (Tables 3 and 5). The percent decrease, $\Delta\sigma_{red}$, of reduced stress in the stretch ratio range from unity to λ_{min} tends to assume values which increase with the HAF carbon black concentration. This behavior is obviously due to filler-cluster formation increasing with filler concentration and resulting in a greater extent of strain-induced filler-cluster breakdown. Such explanation is corroborated by a close correlation of $\Delta\sigma_{red}$ with X_o. Our values of parameter X_o behave in a manner similar to that observed by Luo et al. [8], i.e., they increase with filler concentration. For virgin networks, the network-density-reflecting parameter, C_1, shows a certain tendency to decrease with increasing carbon black concentration, i.e. with the decreasing content of polymer matrix in the system. Luo et al. found an increase in G_c ($\sim C_1$) with filler concentration and assumed the formation of filler–polymer couplings to be responsible [8]. In our case, the low number of data precludes any definite conclusion. The constraint modulus ($2C_2$) of virgin networks shows a distinct tendency to increase with the HAF carbon black concentration, in accord with the observation of Luo et al. of the effect of the ISAF black. Similarly to the findings of Klüppel et al., some values of X_∞ drop below unity (cf. Section 1.2), but even at the highest applied stretch ratio the strain amplifier remains higher than the lowest physically reasonable value of unity.

The energy per unit volume lost in the Mullins softening is given by the area A_{1-3} limited by curves 1 and 3 in Fig. 11. The contribution of filler-cluster breakdown to the Mullins softening is given by the area A_{1-2} limited by curves 1 and 2. The relative contribution of filler-cluster breakdown to the total energy loss, $E_{r,fill} = A_{1-2}/A_{1-3}$ tends to increase with filler concentration (Tables 5 and 6). The exact form of such concentration dependence may be affected by the conditions of comparison (i.e., constant maximum deformation, stress, input energy).

The stress–strain behavior of the SBR 50sil network reinforced with 50 phr of precipitated silica (data in [41]) offers a somewhat different picture (Fig. 13) than that of Fig. 12. The shape of the dependence of $\log(\sigma_{red})$ on λ around its minimum is highly asymmetric and for $\lambda > \lambda_{min}$, the reduced stress increases but slightly. A pronounced decrease in reduced stress at low strains – larger than that found in carbon black-reinforced networks – can be ascribed to a disruption of extensively formed filler–filler structures, as formulated by Bueche [41]. In the approach of Klüppel et al., the term filler-cluster breakdown is used; it manifests itself in a very pronounced strain dependence of the strain-amplification factor (Table 6). As a result, most of the Mullins softening of the SBR 50sil network is due to filler-cluster breakdown (curve 2a) and $E_{r,fill}$ is as high as 85%. Except for one point at the lowest strain, curve 2 drawn with the appropriate values of X_m and $\lambda_{cm,m}$, gives a satisfactory description of the second extension.

Table 6
Parameter values of the ABGILFILpd equation for the SBR 50sil network and curves in Fig. 9; $n = 0.2$

Parameters and properties	Curves					
	1	2a	2	3	4a	4
C_1 (MPa)	0.085	0.085	0.085	0.130	0.130	0.130
C_2 (MPa)	0.245	0.245	0.245	0.250	0.250	0.250
λ_{cm}			5.17_8			2.97_2
X			2.64_8			1.361
$\lambda_{c,a}$	1.50	1.50		1.22	1.22	
$\lambda_{cm,a}$	3.95	3.95		1.72	1.72	
$\lambda_{c,b}$	4.56	4.56		2.66_3	2.66_3	
$\lambda_{cm,b}$	5.17_8	5.17_8		2.97_2	2.97_2	
a	1.02	1.02		1.15	1.15	
X_o	6.15	2.64_8		1.77	1.36_1	
X_∞	0			1.0		
α	1.12			1.0		
$\Delta\sigma_{red}$ (%)	72			26.5		
σ_{red} ($\lambda = 1$) (MPa)	4.13			1.52		
$E_{r,Mull}$ (%)	35					
$E_{r,fill}$ (%)	86					

$\Delta\sigma_{red}$, σ_{red} ($\lambda = 1$), $E_{r,Mull}$, $E_{r,fill}$ – see Tables 3 and 5.

After the second extension–retraction cycle was finished, the specimen was subjected to a heat treatment at 115 °C for 22 h. From the subsequently measured third extension data (open circles), it is observed that, due to heat treatment, the stress at medium and high strains has recovered completely while at low strains the recovery is small. The ABGILFILpd parameters show that after the specimen was strain-softened and subsequently heat-treated, the original highly strain-dependent amplifying factor decreased and became much less strain-dependent. The finite extensibility parameter decreased but its strain dependence ($\lambda_{cm,b} - \lambda_{cm,a}$) remained practically the same. There are some other differences between the original and the softened and subsequently heat-treated network. The parameter C_1 reflecting network density increased by 18% and the finite extensibility parameter at the highest stretch ratio ($\lambda_m = 3.6$) decreased by some 20% with respect to the first extension. Whether the structural processes taking place on heat treatment are of a purely physical character is questionable. One could conjecture that under the given conditions of heat treatment, with no antioxidant added to the compound and with temperature and time of treatment commonly used in tests of accelerated aging, some oxidative crosslinking might have taken place and been responsible for the increase in C_1 and decrease in N. An exposition of a virgin specimen to the conditions of heat treatment could give some comparative information on the molecular background of the observed changes. Also, a further (fourth) extension of the twice extended, heat-treated and thereafter extended specimen might be helpful in giving useful information. The parameter values of the heat-treated specimen predict that the subsequent (i.e., fourth) extension should again produce a softening with respect to the third extension, this time due to the increase in the finite extensibility parameter to its upper limit attained on third extension, and – since clusters have been largely broken down – with a small contribution of the filler.

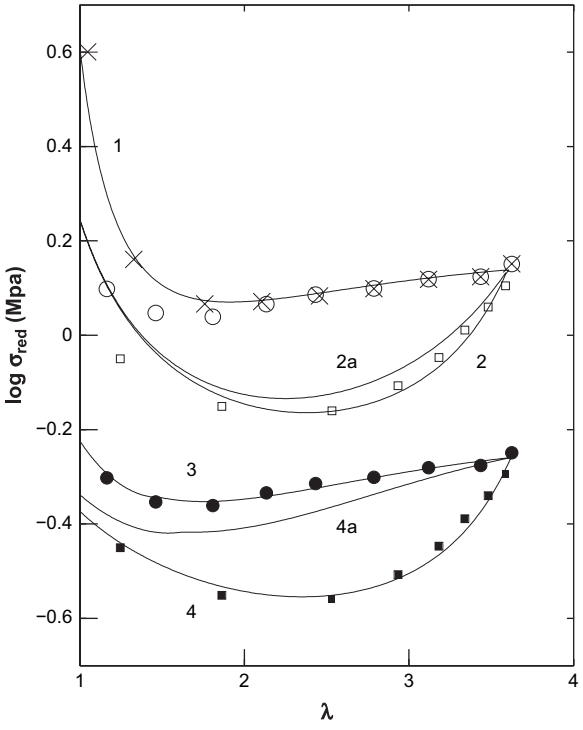

Fig. 13. Comparison of experimental data on the SBR 50sil network [41] with curves drawn according to the ABGILFILpd equation, parameters are in Table 6. First extension: ×, curve 1. Second extension: □. Curve 2a – the same parameters as for curve 1 but X constant. Curve 2 – X, λ_{cm} constant. Third extension after heat treatment: ○ and ●; ● and curve 3 shifted vertically by −0.4. Points ■ equivalent to the second extension but shifted vertically by −0.4. Hypothetical fourth extension: curve 4a – the same parameters as for curve 3 but X constant. Curve 4 – X, λ_{cm} constant.

5. Discussion

As shown in Appendix D, the Edwards–Vilgis approach to the finite network extensibility is not molecularly based and has a phenomenological character. The Klüppel–Schramm treatment is of the same type and, moreover, its prediction for the contribution of finite extensibility to stress at low strains is not physically sound. The main reason for the inability of Eqs. (2)–(5) to correctly represent biaxial data on filler-reinforced networks lies primarily in the inadequacy of the constraint term and not in a failure of the one-mechanism damage model. The Klüppel–Schramm equibiaxial measurements do not seem trustworthy and the use of such data in ''plausibility tests'' of constitutive equations is questionable. The Edwards–Vilgis, Kaliske–Heinrich and Klüppel–Schramm predictions of the stress-upturn behavior fail to describe some important experimental stress–strain dependences.

The ABGIL constitutive equation for homogenous (unfilled) elastomer networks incorporates the two-parameter (C_1, λ_{cm}) connectivity term, the two-parameter (C_2, n) constraint term and a semi-empirical concept of a strain-dependent finite extensibility parameter (network mesh size). By prestraining, the behavior of an SBR network was simplified and the finite extensibility parameter was found to be strain-independent. The parameter values for five hydrocarbon rubber networks (IR, SBR, three NR) were determined previously

[4,5] and their relation to the network and polymer structure was discussed in some detail [5]. The value of $n \approx 0.2$ was the most frequent one. The reduced stress extrapolated to zero strain (the zero-strain shear modulus) $\sigma_{red}(\lambda = 1) = 2C_1 + 2C_2 + FE$, where FE is a contribution of finite extensibility of network chains, which is small for not-too-highly crosslinked networks. The plateau modulus, G_N^0, of the uncrosslinked polymer, given by entanglements, contributes both to the constraint modulus, $2C_2$, and to the connectivity modulus, $2C_1$ [5]. With increase in crosslink concentration, the concentration of network chains ($2C_1$, connectivity modulus) increases and the network chain length (extensibility) decreases, the constraint modulus $2C_2$ being affected to a smaller extent. In order to obtain an acceptable stiffness–extensibility compromise in practical applications, the range of permissible crosslink concentrations cannot be too wide. This is exemplified by the rather narrow ranges of parameter values and zero-strain moduli of three NR networks [22,24,44] crosslinked to different extents (Table 7).

Measurements on two unfilled SBR networks indicate a higher constraint modulus and zero-strain modulus than the corresponding values obtained on NR networks. The difference is obviously due to a higher G_N^0 value (800 kPa) of SBR compared with that of NR (450 kPa) [5].

For filler-reinforced networks, the ABGILpd equation is extended to the ABGILFILpd equation by incorporating the concept of Klüppel and Schramm [3] of a three parameter (X_o, X_∞, α) strain-amplification function based on a one-mechanism model of filler-cluster breakdown; volume changes on strain and permanent set formation are not considered. Similarly to the unfilled networks, the most appropriate value of the exponent n was found to be 0.2. The zero-strain modulus following from the ABGILFILpd equation is related to C_1, C_2, FE, in the same way as the modulus of unfilled networks but it is significantly increased by a factor of X_o:

$$\sigma_{red}(\lambda = 1) = (2C_1 + 2C_2 + FE)X_o$$

As mentioned above, the percent decrease in the reduced stress from $\sigma_{red}(\lambda = 1)$ to its minimum value of $\sigma_{red}(\lambda_{min})$ correlates with X_o. With increasing stretch ratio, the contribution of the constraint term to the reduced stress decreases monotonically while the contribution of the connectivity term passes through a minimum and thereafter increases due to finite extensibility. Data in Table 7 show the effect mentioned above: the constraint modulus tends to increase with filler concentration while the connectivity modulus is less affected. No explanation is available at present for the rather high $2C_1$ of the NR40 prestrained network. The constraint and zero-strain moduli of filler-reinforced SBR networks tend to be higher than those of NR networks, similarly to the unfilled networks. The effect of a higher plateau modulus G_N^0 of SBR obviously plays its role even in the presence of fillers.

A comparison of the ABGILFILpd equation with experimental data strongly suggests that at least two factors contribute to the Mullins strain-softening. At lower strains, the filler-cluster breakdown mainly operates while the contribution of the strain-induced increase in the finite extensibility parameter becomes more pronounced at higher strains. The relative contribution to strain-softening of the first factor tends to diminish with decreasing filler concentration; in the absence of filler, only the second factor contributes – together with the decrease in C_2 – to the strain-softening observed in lightly crosslinked unfilled networks.

In the Göktepe and Miehe model [11], the Mullins-type strain-softening is due to a damage mechanism resulting from the breakdown of chain-particle bonds. On the other hand, Hanson et al. [46] argue that the Miehe mechanism of a permanent material damage as chains are torn loose from the surface of filler particles and the number of network chains is thus reduced, is not compatible with their own experimental observations. They propose a mechanism which conserves the number of network chains, and only the entanglement density with respect to the original strain axis is reduced. Our mechanism of the strain-induced increase in the network mesh size explains the softening by sliding of entanglements at higher strains. Such process is not considered in the Göktepe–Miehe model but is consistent with the Hanson mechanism which considers removal of entanglements associated with the strain axis by one chain sliding under another chain at its attachment point to a filler particle; entanglements associated with strains along axes perpendicular to the first strain would likely not be affected. On the other hand and in contrast to Hanson et al., our data analysis leads to the conclusion that changes at the polymer–filler interface and/or in the matrix cannot be the only sources of softening and that the mechanism of Klüppel and Schramm [3] of strain-induced breakdown of filler clusters is an important contributor. The filler-cluster breakdown is

Table 7
Ranges of parameter values obtained on the studied networks

Parameters and properties	NR unfilled	NR filled virgin	NR filled prestrained	SBR unfilled virgin	SBR unfilled prestrained	SBR filled virgin
No. of networks	3	4	1	2	1	5[a]
Filler concentration (phr)	0	20–69	40	0	0	30–60
n	0.2	0.2	0.2	0.2–0.45	0.2	0.2
$2C_1$ (kPa)	140–300	250–300	390	84–150	90	170–320
$2C_2$ (kPa)	150–220	140–370	200	390–360	205	290–480
N ($=\lambda^2_{cm,b}$)	24–14	8–22	11	34–8.5	34	8–31
σ_{red} ($\lambda = 1$) (kPa)	330–470	800–3700	1200	475–520	300	1200–5200

[a] Includes results on a SBR network containing 60 phr of HAF black [45].

signalized on the first stretching already: it manifests itself in the magnitude of the initial decrease in reduced stress.

A final note should be added. Comparisons of the published theoretical models of the Mullins-type softening with experimental data have practically always been done using linear stress–strain coordinates. In such type of plot, however, the small-strain data are not properly taken into account. The absolute values of the deviations of experimental points from fitted curves become small to negligible at small strains, in spite of their being often rather large *relatively*. A meaningful testing of theoretical predictions requires a detailed knowledge of stress–strain dependences down to very low strains. Comparison of Figs. 11 and 12 shows the advantage and importance of using plots of log *reduced* stress vs strain. Such plots offer a realistic assessment of point-curve deviations and give the low-strain data the appropriate statistical weight in drawing conclusions.

6. Conclusions

Using the proposed ABGILFILpd constitutive equation we have obtained:

1. A very good description of the stress–strain dependences in uniaxial extension of virgin filler-reinforced NR and SBR networks;
2. A very good prediction, based on uniaxial data, of the equibiaxial extension (uniaxial compression), for networks with filler concentrations up to 70 phr, using $n = 0.2$; the value $n = -1$ following from one of the theories [3] was shown previously [4] and again here to lead to non-constitutive predictions;
3. An excellent description of the general biaxial behavior of an NR gum network and a satisfactory biaxial stress–strain data description of the corresponding filler-reinforced prestrain-softened network NR 40;
4. A very good prediction of the magnitude of the Mullins softening from the knowledge of the tensile stress–strain behavior of the respective virgin network. The limiting values, X_m, $\lambda_{cm,m}$, attained at the highest prestrain govern the stress–strain behavior on subsequent extension.

It is concluded that at least two factors contribute to the Mullins softening: at lower strains, the filler-cluster breakdown proposed by Klüppel et al. is the main factor while the strain-induced increase in the network mesh size increasingly contributes at higher strains and plays a role even in the filler absence. The concept of strain-induced increase in the finite extensibility parameter (network mesh size) is consistent with the mechanism of entanglements removal at the matrix–filler interface recently proposed and discussed by Hanson et al. [46].

In derivation of the Edwards–Vilgis, Kaliske–Heinrich and Kluppel–Schramm theories, a step is included which does not follow from structural considerations. It imparts to the respective connectivity terms a phenomenological character and adversely affects their ability to represent the experimental stress-upturn behavior of some important network systems.

Acknowledgement

The authors are greatly indebted to the Grant Agency of the Czech Republic for financial support of this work within the grant project No. 203/05/2252.

Appendix A

The non-affine micro-sphere model. The Miehe theory [6] based on a non-affine micro-sphere (NAMS) model contains five material parameters: μ – effective shear modulus proportional to the network chain density, ν; N – number of chain segments in a network chain; U – tube geometry parameter reflecting constraint stiffness; q – non-affine tube parameter reflecting the shape of the constraint stress; p – non-affine stretch parameter introducing a flexibility of the locking stretch; the Arruda–Boyce eight-chain-model is just a special case with $p = 2$. The NAMS theory was shown [6] to give an excellent description of the well-known stress–strain data of Treloar [44] and of James et al. [22] in uniaxial extension, equibiaxial extension and in pure shear. The James network has a distinctly higher zero-strain modulus than that of Treloar [4,5] and in unfilled networks such observation is commonly ascribed to a higher crosslink concentration. One would expect that data fitting will yield a higher μ for the James et al. network. However, the authors determined equal values of μ (equal network chain densities) for both networks and do not offer any explanation for the finding that the fitted constraint stiffness U of the Treloar network is four times larger and its non-affine tube parameter q six times smaller than that of the James et al. network.

Göktepe and Miehe [11] compared predictions of their model with stress–strain properties of two filler-reinforced networks, denoted here as SBR 30 and SBR 50. Fig. 11 shows that the stress–strain behavior of these two networks does not differ appreciably; we determined similar values for both their connectivity moduli and constraint moduli (Table 5). Göktepe and Miehe determined moduli, μ^{cc}, of the crosslink-to-crosslink network and found values differing by a factor of four, 0.11 and 0.41 MPa, respectively. The values obtained for the constraint parameter, U (2.03 and 0.53) also differ by a factor of four. No interpretation of these results is given in the original paper [11] thus leaving the impression that the obtained parameter values are rather of a phenomenological character.

Appendix B

Stress–strain relations ((8) and (10)) can be written in the general form

$$\sigma_i = A_1\left(\lambda_i^2 - \lambda_3^2\right)/\lambda_i + A_2\left(\lambda_i^n - \lambda_3^n\right)/\lambda_i \qquad \text{(B.1)}$$

The meaning of A_1, A_2 follows from a comparison of Eq. (B.1) with Eq. (8) or (10).

Special cases of Eq. (B.1) for the most often used geometrical modes are the following

Stress in uniaxial extension UE

$$\lambda_3 = \lambda_2 = 1/\lambda_1^{1/2}; \quad \lambda_c = \left(\left(\lambda_1^2 + 2/\lambda_1\right)/3\right)^{1/2}$$

$$\sigma_1 = A_1\left(\lambda_1 - 1/\lambda_1^2\right) + A_2\left(\lambda_1^{n-1} - 1/\lambda_1^{(1+n/2)}\right); \quad \sigma_2 = 0 \tag{B.2}$$

Stress in equibiaxial extension EBE

$$\lambda_1 = \lambda_2; \quad \lambda_c = \left(\left(2\lambda_1^2 + 1/\lambda_1^4\right)/3\right)^{1/2}$$

$$\sigma_1 = A_1\left(\lambda_1 - 1/\lambda_1^5\right) + A_2\left(\lambda_1^{n-1} - 1/\lambda_1^{(1+2n)}\right); \quad \sigma_2 = \sigma_1 \tag{B.3}$$

Stresses in pure shear PS

$$\lambda_2 = 1; \quad \lambda_3 = 1/\lambda_1; \quad \lambda_c = \left(\left(\lambda_1^2 + 1 + 1/\lambda_1^2\right)/3\right)^{1/2}$$

longitudinal pure shear stress PS1

$$\sigma_1 = A_1\left(\lambda_1 - 1/\lambda_1^3\right) + A_2\left(\lambda_1^{n-1} - 1/\lambda_1^{(1+n)}\right) \tag{B.4}$$

transverse pure shear stress PS2

$$\sigma_2 = A_1\left(1 - 1/\lambda_1^2\right) + A_2\left(1 - 1/\lambda_1^n\right) \tag{B.5}$$

Appendix C

In the range of x from 0.7 to 0.9, the relative difference $D = L_{pd}^{-1}(x) - L^{-1}(x)/L^{-1}(x)$ between the Padé approximation, $L_{pd}^{-1}(x)$, and the inverse Langevin function, $L^{-1}(x)$, approaches 5%, otherwise it is smaller than 3.5%:

x	0.2	0.4	0.6	0.7	0.8	0.85	0.90	0.95	0.98
D (%)	0.3	1.2	3.1	4.28	4.90	4.64	3.74	2.20	0.95

With x decreasing below 0.2, D drops to zero.

Appendix D

Comments on the Edwards–Vilgis approach to the finite network extensibility.

Citation from our previous paper [47], p. 3807:

It should be noted that for the end-to-end distance distribution of a tube-like confined network chain, Edwards and Vilgis [1] intentionally chose a simple empirical function; they write: ''How can we model the singularity in entropy? There are many possible models (including of course *the exact Langevin*) but we want a representation which is amenable to calculation and contains the essential features of inextensibility.'' Thus, both the crosslinking term of the Edwards–Vilgis free energy and the calculated stresses based on it are to be looked upon as mere phenomenological approximations of a conceivable rigorous treatment that would model the singularity in chain entropy using Langevin statistics. Such calculation would probably lead to a function more resembling the result derived by Arruda and Boyce.

Further arguments: Let σ be the stress calculated for the connectivity term in the frame of the Edwards–Vilgis theory [1] and σ_{Gauss} the stress calculated in the frame of the Gaussian theory. The relative stress contribution of finite extensibility, FE_{rel}, to the Gaussian stress is expressed by

$FE_{rel} = (\sigma/\sigma_{Gauss}) - 1$, and from the Edwards–Vilgis theory [1] one gets

$$FE_{rel} = \frac{1 - \left(2d - d^2 I_1\right)}{1 - I_1\left(2d - d^2 I_1\right)} - 1 \tag{D.1}$$

where d is the inextensibility parameter ($d = 0$ for infinite extensibility) and $I_i = \sum_i \lambda_i^2$. At small strains approaching zero, $I_1 \approx 3$, and for $d > 0$ the expression for FE_{rel} is seen to be non-zero and positive, as expected. With increasing strain, FE_{rel} increases.

The Kaliske–Heinrich and Klüppel–Schramm FE_{rel} can formally be expressed by the same Eq. (D.1) where, however, I_1 is replaced by $I_m = I_1 - 3$ (see Eq. (2)). For $d > 0$ and $I_1 \approx 3$, one gets $I_m \approx 0$, and the relative contribution of finite extensibility to the Gaussian stress can be deduced from Eq. (D.1) as

$$FE_{rel} = -2d \tag{D.2}$$

FE_{rel} is now predicted to be non-zero and *negative*. Such result, of course, is not physically realistic and casts doubts on the Kaliske–Heinrich and Klüppel–Schramm treatments. For example, if $\sum_i \lambda_i^2 \approx 3$ and $d = 0.02$, then the Edwards–Vilgis finite extensibility contribution to the Gaussian stress amounts to +8.8% whereas that of Klüppel and Schramm to −4%; the difference ≈13% is small but not negligible. The Kluppel–Schramm value of FE_{rel} does not become higher than zero before I_1 exceeds 4 (i.e., in uniaxial extension, if λ_1 exceeds 1.67); with further increasing strain it approaches the Edwards–Vilgis FE_{rel}.

References

[1] Edwards SF, Vilgis TA. Polymer 1986;27:483–92.
[2] Kaliske M, Heinrich G. Rubber Chem Technol 1999;72:602–32.
[3] Klüppel M, Schramm J. Macromol Theory Simul 2000;9:742–54.
[4] Meissner B, Matějka L. Polymer 2003;44:4599–610.
[5] Meissner B, Matějka L. Polymer 2004;45:7247–60.
[6] Miehe C, Göktepe S, Lulei F. J Mech Phys Solids 2004;52:2617–60.
[7] Heinrich G, Klüppel M, Vilgis TA. Curr Opin Solid State Mater Sci 2002;6:195–203.
[8] Luo H, Klüppel M, Schneider H. Macromolecules 2004;37:8000–9.

[9] Mullins L, Tobin NR. Rubber Chem Technol 1957;30:555–71.
[10] Bueche F. J Appl Polym Sci 1960;15:271–81.
[11] Göktepe S, Miehe C. J Mech Phys Solids 2005;53:2259–83.
[12] Klüppel M, Menge H, Schmidt H, Schneider H, Schuster RH. Macromolecules 2001;34:8107–16.
[13] James HM, Guth E. J Chem Phys 1943;11:455–81.
[14] Klüppel M. Prog Colloid Polym Sci 1992;90:137–43.
[15] Klüppel M. J Appl Polym Sci 1993;48:1137–50.
[16] Klüppel M, Heinrich G. Macromolecules 1994;27:3596–603.
[17] Klüppel M. Macromolecules 1994;27:7179–84.
[18] Klüppel M, Meier J. In: Besdo D, Schuster RH, Ihleman J, editors. Constitutive models for rubber II. Lisse: Balkema; 2001.
[19] Klüppel M, Meier J, Heinrich G. In: Busfield JJC, Muhr GAH, editors. Constitutive models for rubber III. Lisse: Balkema; 2003.
[20] Klüppel M, Meier J, Dämgen M. In: Austrell P-E, Kari L, editors. Constitutive models for rubber IV. London: Taylor and Francis Group; 2005.
[21] Klüppel M. Adv Polym Sci 2003;164:1–86.
[22] James AG, Green A, Simpson GM. J Appl Polym Sci 1975;19:2033–58.
[23] James AG, Green A. J Appl Polym Sci 1975;19:2319–30.
[24] Rivlin RS, Saunders DW. Philos Trans R Soc London Ser A 1951; 243:251–88.
[25] Meissner B. Polymer 2000;41:7827–41.
[26] Meissner B, Matějka L. Polymer 2001;42:1143–56.
[27] Arruda EM, Boyce MC. J Mech Phys Solids 1993;41:389–412.
[28] Heinrich G, Straube E. Acta Polym 1983;34:589–94.
[29] Gaylord RJ, Douglas JF. Polym Bull 1987;18:347–54.
[30] Gaylord RJ, Douglas JF. Polym Bull 1990;23:529–33.
[31] Rubinstein M, Panyukov S. Macromolecules 1997;30:8036–44.
[32] Rubinstein M, Panyukov S. Macromolecules 2002;35:6670–86.
[33] Heinrich G, Straube E, Helmis G. Adv Polym Sci 1988;85:33–87.
[34] Cohen A. Rheol Acta 1991;30:270–3.
[35] Mooney M. J Appl Phys 1940;11:582–92.
[36] Rivlin RS. Philos Trans R Soc London Ser A 1948;241:379–97.
[37] Meissner B, Matějka L. Polymer 2000;41:7749–60.
[38] Wu PD, van der Giessen E. J Mech Phys Solids 1993;41:427–56.
[39] Meissner B, Matějka L. Polymer 2003;44:4611–7.
[40] Davies CKL, De DK, Thomas AG. Rubber Chem Technol 1994;67:716–28.
[41] Bueche F. J Appl Polym Sci 1961;2:271–81.
[42] Harwood JAC, Mullins L, Payne AR. J Appl Polym Sci 1965;9:3011–21.
[43] Kilian HG, Strauss M, Hamm W. Rubber Chem Technol 1994;67:1–16.
[44] Treloar LRG. Trans Faraday Soc 1944;40:59–70.
[45] Ambacher H, Strauss M, Kilian HG, Wolff S. Kautsch Gummi Kunstst 1991;44:1111–8.
[46] Hanson DE, Hawley M, Houlton R, Chitanvis K, Rae P, Orler BE, et al. Polymer 2005;46:10989–95.
[47] Meissner B, Matějka L. Polymer 2002;43:3803–9.